

Free Your Hands: Lightweight Relightable Turntable Capture Pipeline

JIAHUI FAN, Nanjing University of Science and Technology, China

FUJUN LUAN, Adobe Research, USA

JIAN YANG[†], Nanjing University of Science and Technology, China

MILOŠ HAŠAN, Adobe Research, USA

BEIBEI WANG[†], Nanjing University, China

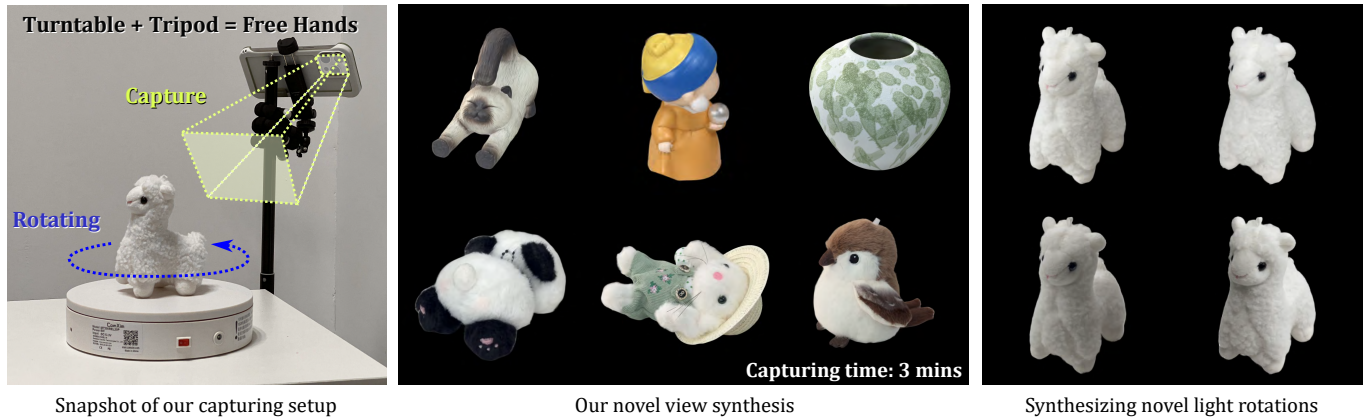


Fig. 1. We present a lightweight object-capturing pipeline to reduce the workload and standardize the acquisition procedure. We use a consumer turntable to carry the object and a tripod to hold the camera (left), automatically capturing dense samples from various views and lighting conditions. This way, we easily obtain hundreds of high-quality captures within 3 minutes. We develop a conditional neural radiance representation, achieving high-quality novel view synthesis (middle). With this representation, we can further synthesize results under novel views and light rotations (right).

Novel view synthesis (NVS) from multiple captured photos of an object is a widely studied problem. Achieving high quality typically requires dense sampling of input views, which can lead to frustrating and tedious manual labor. Manually positioning cameras to maintain an optimal desired distribution can be difficult for humans, and if a good distribution is found, it is not easy to replicate. Additionally, the captured data can suffer from motion blur and defocus due to human error. In this paper, we present a lightweight object capture pipeline to reduce the manual workload and standardize the acquisition setup. We use a consumer turntable to carry the object and a tripod to hold the camera. As the turntable rotates, we automatically capture dense samples from various views and lighting conditions; we can repeat this for several camera positions. This way, we can easily capture hundreds of valid images in several minutes without hands-on effort. However, in the object reference frame, the light conditions vary; this is harmful to a standard NVS method like 3D Gaussian splatting (3DGS) which assumes fixed lighting. We design a neural radiance representation conditioned on light rotations, which addresses this issue and allows relightability as an additional benefit. We demonstrate our pipeline using 3DGS as the underlying framework, achieving competitive quality compared to previous methods with exhaustive acquisition and showcasing its potential for relighting and harmonization tasks.

[†]Corresponding authors. Email: csjiang@nju.edu.cn.

[†]Corresponding authors. Email: beibei.wang@nju.edu.cn.

Authors' addresses: Jiahui Fan, Nanjing University of Science and Technology, China, fjh@nju.edu.cn; Fujun Luan, Adobe Research, USA, fluan@adobe.com; Jian Yang[†], Nanjing University of Science and Technology, China, csjiang@nju.edu.cn; Miloš Hašan, Adobe Research, USA, milos.hasan@gmail.com; Beibei Wang[†], Nanjing University, China, beibei.wang@nju.edu.cn.

1 INTRODUCTION

Creating realistic 3D digital assets from real-world objects is a long-standing challenge of computer graphics, with applications to e-commerce, entertainment, digital heritage and more. A typical pipeline captures multiple views of an object under fixed lighting and transforms the captured images into a 3D digital asset, which allows novel view synthesis (NVS) or in some cases, relighting. Neural radiance fields (NeRF) [Mildenhall et al. 2021] or 3D Gaussian splatting (3DGS) [Kerbl et al. 2023] can be used for this purpose, but high-quality photograph capture still requires careful manual labor and time, as these methods require fairly dense views (typically hundreds). Handheld camera videos are faster to capture but frequently suffer from motion blur and defocus.

Images can also be captured with specialized devices [Kang et al. 2023; Ma et al. 2021; Ye et al. 2024]; this can reduce the required human labor and precision, but these devices are often not easily accessible, limiting their applicability. In the case of hand-held cameras, various lighting setups can be employed, including unknown environment lighting [Wang et al. 2021; Zhang et al. 2020], or a point light that is collocated with the camera [Bi et al. 2020a,b,c], or separate from the camera [Bi et al. 2024a; Gao et al. 2020]. In all cases, the camera is held by a human hand. The constraints on a reasonable sampling of viewpoints may be obvious to researchers, but manually positioning cameras to maintain the desired distribution can be difficult for average users. Additionally, the quality of captured data can suffer from issues like motion blur and defocus, as shown

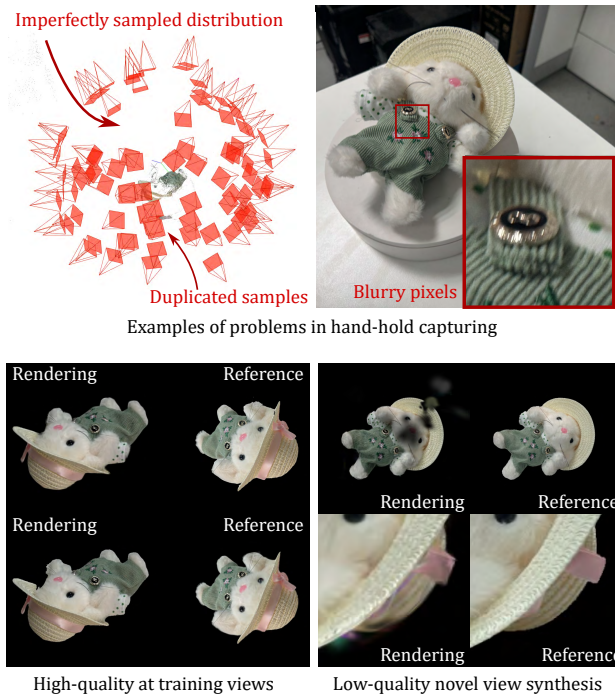


Fig. 2. Illustrations of some common problems in the ordinary hand-held capturing pipeline. The final NVS quality can suffer from the imperfectly sampled distribution and blurry images.

in Fig. 2. Several works propose utilizing sparse views and cross-scene feed-forward inference techniques [Charatan et al. 2024; Chen et al. 2025]. However, the reconstructed quality necessarily degrades without dense samples.

In this paper, we present a lightweight object capture pipeline designed to reduce manual workload, standardize the acquisition process and make it repeatable, while also obtaining some relightability as an additional benefit. We use a consumer turntable to carry the object and a tripod to support the camera. As the turntable rotates, we automatically capture dense samples from various views and under different lighting conditions (i.e., rotating environment light as observed from the object’s frame of reference). This way, we can easily capture hundreds of valid images in several minutes without hands-on effort, while minimizing issues with blur and defocus. The captured images can be used in existing NVS frameworks (NeRF or 3DGS). However, the varying light conditions break the assumptions of these techniques, and are harmful to the reconstruction quality. Therefore, we design a radiance representation conditioned on light rotations to bridge the gap.

We first discuss the insights behind our turntable design from a theoretical perspective. Next, we demonstrate our pipeline using 3DGS as the underlying framework, achieving competitive quality compared to previous methods with exhaustive acquisition, while also showcasing potential for relighting and harmonization tasks. To summarize, our main contributions include:

- a novel lightweight capture pipeline that uses a turntable and tripod to minimize manual workload and standardize the acquisition process,
- a rotation-conditioned radiance field representation tailored for our capture pipeline and allowing relightability in the form of lighting rotation, and
- a dataset consisting of glossy and furry objects captured and reconstructed under different lighting configurations with our pipeline, available for downstream research.

2 RELATED WORK

Novel view synthesis. Novel view synthesis (NVS) aims to generate new images from view directions that were not originally observed. Extensive research on 3D representations has been proposed to enable realistic novel view rendering. Notably, NeRF [Mildenhall et al. 2021], 3DGS [Kerbl et al. 2023] and their follow-ups have garnered significant attention due to their powerful representation capabilities.

NeRF models radiance using integrals over a ray passing through a volume, and addresses view-dependent radiance using multilayer perceptrons (MLPs) conditioned on the view ray direction; this is also true in most follow-up methods [Chen et al. 2022; Müller et al. 2022]. Enhanced anti-aliasing techniques [Barron et al. 2021, 2022, 2023; Zhang et al. 2020] and improved reflectance modeling [Attal et al. 2023; Verbin et al. 2022] have further refined the quality and performance of NeRF-based representations. 3DGS [Kerbl et al. 2023] employs anisotropic Gaussians to represent scenes, allowing for great adaptivity to actual geometric content and enabling real-time, highly detailed renderings. The view dependence of radiance is represented using spherical harmonics, which is even more limited than MLP-based view-dependence.

Inverse rendering and relighting. Based on these NVS frameworks, some inverse rendering approaches [Bi et al. 2020a; Boss et al. 2021; Jin et al. 2023; Liang et al. 2024; Liu et al. 2023; Yao et al. 2022; Zhang et al. 2021] allow for the relighting with novel environment lights by decomposing the light, material and geometry of the target object. Gao et al. [2020] leverage a learned neural texture on a rough proxy geometry to achieve relighting of objects. Mullia et al. [2024] propose a novel representation that combines explicit geometry with a neural feature grid and an MLP decoder, achieving high-fidelity rendering and relighting with good flexibility and integration. NRHints [Zeng et al. 2023] maintains an implicit neural representation with both SDF and NeRF and predicts radiance with shadow and highlight hints, achieving high-quality relighting. With 3DGS as the framework, some work [Bi et al. 2024b; Gao et al. 2023] also relight objects with analytical appearance approximation or neural appearances. These approaches decompose the illumination and materials from the object, supporting arbitrary novel environments or point lights with full relightability, but at the cost of introducing limited material models and often baking lighting features into material properties. Compared to these methods, we opt for a simpler way without explicitly modeling the illumination, achieving partial relighting with rotated or linearly combined environments.

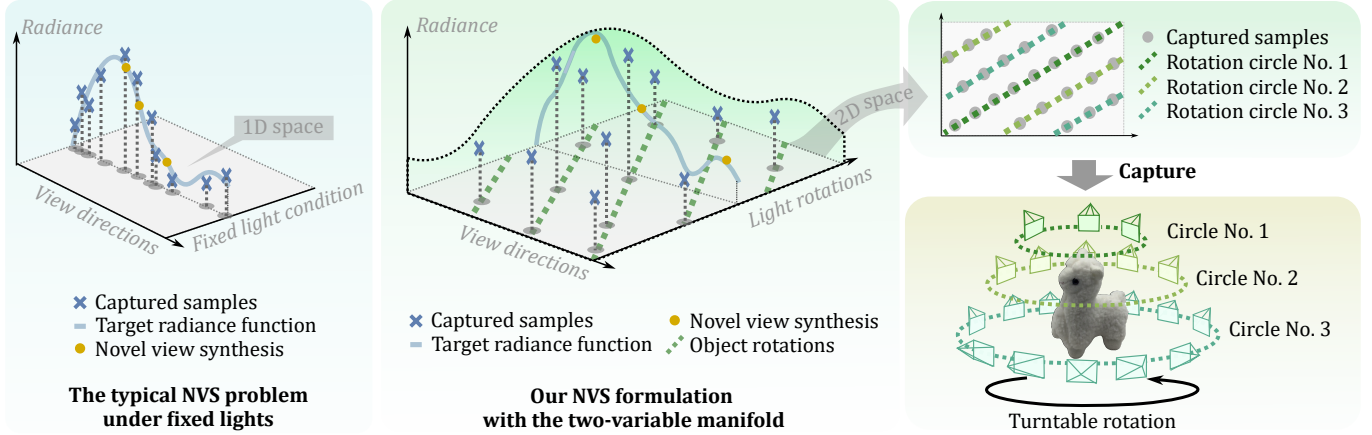


Fig. 3. Intuitively, varying view directions and light rotations can be thought of as a 2-dimensional space of variation. The typical NVS problem (left) can be seen as sampling a single 1D “column” in this space. In our formulation (middle) and its planar projection (right), we use a turntable setup to easily obtain samples along the “diagonal lines” in this two-variable sample space. We capture multiple circles as shown in the right sub-figure, and each circle makes up an orbit of cameras, leading to a continuous and uniform sampling of viewpoints. We fit a manifold to these samples, enabling us to render novel views as well as light rotations; as a consequence, we can finally solve the NVS problem in a specific 1D slice of this manifold.

Camera pose calibration. These above techniques rely on posed images to densely reconstruct 3D scenes, with the quality of the input images significantly influencing the final rendering results. Structure from Motion (SfM) methods [Hartley and Zisserman 2003; Mur-Artal et al. 2015; Schonberger and Frahm 2016; Taketomi et al. 2017], particularly COLMAP [Schönberger and Frahm 2016], are commonly employed to calibrate camera poses and provide initialization for point-based techniques. Although the quality of input data is typically assumed to be sufficient for COLMAP to succeed, this assumption is frequently invalid. Consequently, standardizing the data acquisition process and minimizing human error is beneficial to ensure robust and reliable performance in NVS applications.

3 OUR METHOD

To create a 3D asset from a real-world object for novel view synthesis, a common approach is to capture hundreds of images by moving the camera around the object under a static light condition and then reconstruct the radiance field with NeRF or 3DGS. The entire pipeline can be formulated as follows:

$$L = \mathcal{G}(\mathbf{V}_s, I_0), \quad (1)$$

where L represents the radiance field, \mathcal{G} denotes a reconstruction operator, which can be either NeRF or 3DGS. \mathbf{V}_s is a set of camera views parameterized by the camera intrinsics and extrinsics. I_0 is an arbitrary *static* lighting (illumination) setting (e.g., unknown environment) under which the images are captured.

To ensure high-quality reconstruction, it is necessary to have a dense set of samples, typically hundreds of camera views, leading to manual labor and high possibility of human error. Can we free our hands while maintaining high-quality reconstruction? To answer this challenge, we introduce a novel capture pipeline, presented below.

3.1 Capturing with a turntable

In addition to moving the camera, we can also move or rotate the object itself. A simple yet effective solution to this issue is to use a turntable to hold the object, allowing it to rotate automatically. We can position the camera on a tripod in a small number of locations, to easily capture hundreds of images.

Suppose that the camera is placed at M different locations. For each camera location, a sequence of images corresponding to a full turntable rotation forms a *circle* of N camera positions in the object frame. Unlike the typical capture pipeline, the images are captured under different light conditions when thinking in the object frame of reference: the same lighting environment is rotated differently with respect to the object. This leads to our conditional radiance field reconstruction formulation:

$$L = \mathcal{G}(\mathbf{V}, \mathbf{I}), \quad (2)$$

$$\{\mathbf{V}\} = \{\mathbf{V}_i | i = 0, 1, \dots, M\}, \quad (3)$$

$$\{\mathbf{I}\} = \{\mathbf{I}_j | j = 0, 1, \dots, N\}, \quad (4)$$

where \mathbf{V} consists of samples from M circles captured by placing the camera around the turntable at different elevation and azimuth angles. Here each \mathbf{V}_i is a set of views from one circle, and \mathbf{I} is a set of lighting rotations rather than a static lighting (I_0 in Eqn. (1)). We choose N rotations (\mathbf{I}_j) from each circle, resulting in a total of $M \times N$ samples.

With this setup, we can easily capture hundreds of images with minimum human labor. The remaining question is how to reconstruct the conditional radiance field with these captured images.

3.2 Radiance field reconstruction with varying lighting conditions

The original formulation for radiance field reconstruction, as presented in Eqn. (1), essentially operates as a one-variable regression problem, predicting radiance values from different viewpoints. In

contrast, our conditional radiance field reconstruction approach incorporates a rotating light environment (in object frame), making it a regression problem involving two variables. The key insight behind our formulation is to construct a field conditioned on the two-variable sample space and interpret the NVS problem as a one-dimensional slice of this field, as illustrated in Fig. 3.

We use 3DGS as our underlying 3D representation, though NeRF formulations could be used with small modifications as well. In standard 3DGS, radiance is represented using spherical harmonics (SH) basis functions. While SH vectors are a compact way to represent angular distributions, there is no option to make them conditional on varying light conditions. Instead, we replace per-Gaussian SH representation with a neural network conditioned on light rotations (in addition to view directions) and build the manifold in a neural latent space.

Specifically, each Gaussian has an appearance latent feature vector representing the observed color from given views and light rotations. This appearance latent vector is interpreted by an MLP to decode the conditional radiance field. The color per Gaussian is computed as:

$$c = \text{MLP}(x|v, \theta), \quad (5)$$

where x is the latent vector stored in each Gaussian point, v is the view direction (a normalized 3D direction), and θ is the azimuthal rotation angle. Specifically, the MLP is 128-channel with 2 hidden layers, using a level-2 frequency encoding for the input view directions and light rotations. The latent vectors are 8-dimensional. We evaluate the network before splatting the Gaussians, and the final pixel colors are computed using standard 3DGS differentiable rasterization.

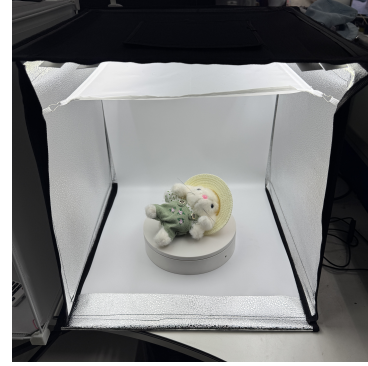
3.3 Applications of our capture pipeline

Our capture pipeline can be applied to various scenarios. Here, we outline several of these applications.

NVS and relighting with the neural radiance representation. One obvious application of our pipeline is for NVS, as stated in the previous section, by computing the radiance for each Gaussian using its latent vectors and performing the alpha-blending. Additionally, since our neural presentation is defined by all different light rotations, it naturally facilitates relighting under all rotating light conditions.

NVS with a distilled SH representation. Besides using the neural representation directly, it can be distilled into other representations (e.g., SHs) by fixing a light rotation angle. The distilled representation allows novel view synthesis, while being compatible with existing 3DGS-based applications.

Relighting under novel light conditions. Since our neural representation encodes the radiance field with multiple light conditions, we can relight the object by linearly combining different light rotations (e.g., front-lit and back-lit ones), achieving a novel light condition. Furthermore, if the original environment lighting is known, it is possible to approximately fit a target lighting using the known rotations, in order to achieve even more complex relighting tasks.



An alternative capturing setup with a studio box

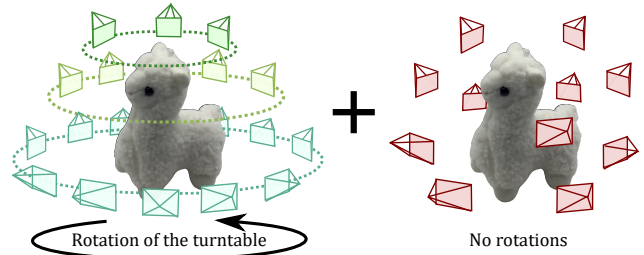


Illustration of extra sparse static captures

Fig. 4. The illustration of some alternative versions of our datasets. The users can easily extend the setup of our pipeline with their desired extensions without obviously increasing the workload and time cost. We showcase and discuss the *extra sparse static captures* setup in our supplementary.

4 IMPLEMENTATION DETAILS

Turntable capture dataset. We have constructed a dataset of turntable captures under various indoor lighting conditions. The dataset consists of 17 real-world objects with diffuse, furry, or glossy appearances. Each object is sampled using $M = 8$ turntable videos featuring different camera elevations and azimuths, and we select $N = 60$ frames from each video, resulting in a total of 480 images for each training set. Another 60 frames from a video at a novel view is used as the testing set. A typical capture process takes 3 minutes.

Our pipeline is flexible and allows for the use of controlled photographic studio lighting or additional camera samples. We offer a version of our dataset captured under a studio light box that delivers controllable soft lighting. Such extensions can enhance the result quality and repeatability, while maintaining the efficiency and simplicity of our pipeline. We describe the *studio box* variant in Fig. 4 and validate it in Sec. 5. We also provide another variation with 20 extra views captured under static lighting, and we discuss it in our supplementary.

Capturing details and data preparation. We show a snapshot of our capturing environment in Fig 12. We use the 48 mm video camera from an iPhone 15 Pro Max and crop the images to get a resolution of 1440×1440 pixels. During capturing, we position the camera approximately every 0.25π radians around the object to

create 8 video sequences, while uniformly varying elevation angles. For the *studio box* case, we only sample viewpoints from the front side of the box, since the object is blocked from other sides.

After capturing, we compute optical flow to identify the start and end points of each rotation cycle (though of course we could also manually stop and restart the videos). We randomly select 60 frames from each cycle. The turntable rotates at a fixed angular velocity, so we divide 2π by the total number of frames to determine the rotation angle at each selected timestamp. All images are masked and the background is automatically removed using SAM2 [Ravi et al. 2024]. We then conduct calibration using COLMAP [Schönberger and Frahm 2016].

Optimization. During optimization, we back-propagate the gradient to the MLP weights, feature vectors and Gaussian parameters. The network weights and the latent vectors are jointly updated and optimized to fit the appearance under the rotating light conditions with L_1 loss function and the structural similarity index (SSIM) [Wang et al. 2004].

5 RESULTS

5.1 Experiment setup

We validate our pipeline on our captured and synthetic datasets. We run all experiments on an Ubuntu 22.04 LTS distribution powered by Windows Subsystem Linux 2. All renderings are done with 800×800 resolution, and training our pipeline typically takes about 15 minutes on an RTX4090 GPU. We evaluate the peak signal-to-noise ratio (PSNR), SSIM, and perceptual similarity (LPIPS) [Zhang et al. 2018] values to compare both the pixel-wise accuracy and global degree of realism.

5.2 Datasets and baseline

We run experiments on our captured real-world datasets and synthesized datasets. As stated in Sec. 4, we provide two versions of our dataset with different capturing setups: (a) using the turntable only (called the *default* dataset) and (b) using an additional studio box for soft lighting (called the *studio box* dataset). We evaluate the NVS and relighting qualities on both datasets in this section. Note that in both datasets, each image is with different views and light rotation angles. We build synthetic data with a simulated turntable only to validate the NVS quality. In the synthetic dataset, all training images are with light rotations but testing images, and we generate ideally sampled fully static images for 3DGS to compare with.

We use 3DGS [Kerbl et al. 2023] as our baseline for comparison. Since other advanced approaches [Liu et al. 2024; Meng et al. 2024; Yu et al. 2024] that enhance 3DGS are orthogonal to our pipeline, we did not perform comparisons with these methods.

5.3 Quality validation

To validate the effectiveness of our pipeline, we compare the rendering quality between our conditional radiance representation and 3DGS on *default* and *studio box* datasets, where quantitative results are provided in Table 1 and the visual comparisons are provided in Figs. 8 and 10. Generally, the *studio box* datasets give a higher rendering quality, since the softened light makes it easier for

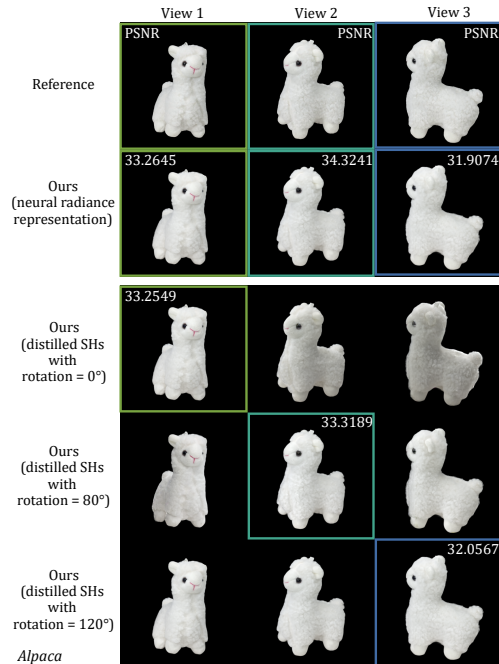


Fig. 5. The NVS result with SHs distilled from our trained model. By a simple distillation process, our conditional radiance representation can be exported into a static radiance field at a specific light rotation angle for simple NVS and easy cooperation with other applications.

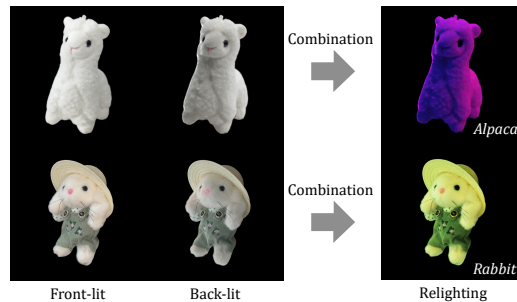


Fig. 6. Relighting the objects by linear combinations of light rotations with RGB weights. Top: blue and purple light combined. Bottom: yellow and green light combined.

both our method and 3DGS to represent the radiance. Our method outperforms 3DGS on both datasets, showing ~ 32 dB on the *default* dataset and ~ 37 dB on the *studio box* dataset.

Default dataset. In Fig. 8, we provide the visual comparison between our method and 3DGS across three scenes selected from the *default* datasets. These scenes include typical complex fur and reflections. By comparison, we find that our method has a much higher quality (about +5 dB) consistently. In particular, 3DGS exhibits an overly dark appearance at grazing angles and obvious blurriness on the furry surface as it cannot handle rotating light conditions.

Table 1. The rendering quality of our neural radiance representation and 3DGS with novel views and light rotations on our captured datasets (both *default* and *studio box*). The results are evaluated in PSNR (\uparrow), SSIM (\uparrow) and LPIPS (\downarrow). The best/second-best results are colored in red / orange. The soft light from the studio box generally provides higher qualities, while the capturing workload stays the same. Our neural radiance representation outperforms 3DGS on both variants of datasets.

| Scene | Default dataset (3 minutes) (Fig.8) | | | | | | Studio box dataset (3 minutes) (Fig.10) | | | | | |
|------------|-------------------------------------|--------|--------|---------|--------|--------|-----------------------------------------|--------|--------|---------|--------|--------|
| | Ours | | | 3DGS | | | Ours | | | 3DGS | | |
| | PSNR | SSIM | LPIPS | PSNR | SSIM | LPIPS | PSNR | SSIM | LPIPS | PSNR | SSIM | LPIPS |
| Alpaca | 33.7039 | 0.9894 | 0.0169 | 29.6081 | 0.9806 | 0.0323 | 34.0134 | 0.9896 | 0.0184 | 31.7581 | 0.9830 | 0.0344 |
| Cat | 30.9368 | 0.9835 | 0.0109 | 26.0663 | 0.9555 | 0.0356 | 40.8780 | 0.9938 | 0.0046 | 35.4237 | 0.9818 | 0.0133 |
| China | 34.2610 | 0.9897 | 0.0090 | 30.7809 | 0.9844 | 0.0146 | 39.6296 | 0.9956 | 0.0052 | 36.5625 | 0.9933 | 0.0084 |
| Controller | 30.4726 | 0.9761 | 0.0209 | 25.2222 | 0.9659 | 0.0345 | 35.4382 | 0.9920 | 0.0089 | 33.0897 | 0.9856 | 0.0180 |
| Dinosaur | 36.0936 | 0.9928 | 0.0065 | 32.5989 | 0.9883 | 0.0123 | 41.9424 | 0.9967 | 0.0045 | 38.4615 | 0.9934 | 0.0097 |
| Dolphin | 39.0878 | 0.9961 | 0.0048 | 34.1935 | 0.9924 | 0.0086 | 42.5473 | 0.9972 | 0.0041 | 40.2936 | 0.9953 | 0.0075 |
| Jar | 29.3733 | 0.9553 | 0.0484 | 23.6761 | 0.9101 | 0.1196 | 33.1215 | 0.9772 | 0.0193 | 28.8963 | 0.9415 | 0.0798 |
| Monza | 36.5302 | 0.9926 | 0.0054 | 29.6788 | 0.9844 | 0.0104 | 41.3471 | 0.9964 | 0.0034 | 38.6690 | 0.9926 | 0.0077 |
| Panda | 29.1212 | 0.9780 | 0.0288 | 25.7316 | 0.9628 | 0.0525 | 36.3338 | 0.9783 | 0.0112 | 32.5720 | 0.9614 | 0.0266 |
| Pearl | 38.0879 | 0.9917 | 0.0070 | 30.4644 | 0.9834 | 0.0140 | 41.4716 | 0.9960 | 0.0045 | 37.4667 | 0.9916 | 0.0105 |
| Penguin | 28.9595 | 0.9698 | 0.0290 | 23.9183 | 0.9453 | 0.0598 | 35.2508 | 0.9792 | 0.0194 | 33.0846 | 0.9571 | 0.0456 |
| Pine | 25.6992 | 0.9451 | 0.0421 | 21.7535 | 0.8820 | 0.0881 | 32.1439 | 0.9724 | 0.0184 | 28.0977 | 0.9354 | 0.0580 |
| Rabbit | 31.6668 | 0.9760 | 0.0200 | 29.4303 | 0.9592 | 0.0413 | 34.1400 | 0.9842 | 0.0191 | 30.5215 | 0.9648 | 0.0413 |
| Rider | 28.6987 | 0.9486 | 0.0345 | 25.3948 | 0.9275 | 0.0535 | 34.9932 | 0.9816 | 0.0190 | 32.7340 | 0.9640 | 0.0378 |
| RiderSmall | 37.5932 | 0.9924 | 0.0053 | 31.0377 | 0.9830 | 0.0115 | 41.9490 | 0.9961 | 0.0055 | 38.5647 | 0.9917 | 0.0105 |
| Sparrow | 29.7554 | 0.9720 | 0.0309 | 25.6735 | 0.9593 | 0.0531 | 31.9495 | 0.9585 | 0.0132 | 31.1654 | 0.9526 | 0.0260 |
| Tuan | 31.5752 | 0.9827 | 0.0234 | 23.9322 | 0.9693 | 0.0439 | 34.6477 | 0.8956 | 0.0087 | 25.7017 | 0.8694 | 0.0277 |
| Average | 32.4968 | 0.9785 | 0.0202 | 27.4832 | 0.9609 | 0.0403 | 37.1645 | 0.9812 | 0.0110 | 33.7096 | 0.9679 | 0.0272 |

Table 2. The comparison of NVS qualities on synthetic datasets. All results are evaluated in PSNR (\uparrow) and LPIPS (\downarrow), and best/second-best results are marked in red / orange. Note that in this comparison, the testing set is without any light rotations. Our method produces higher-quality results from training images with rotating lights than 3DGS does with common dataset setups (100 static images). Even with fairly sufficient ideally sampled static samples, our results are still competitive with them.

| Scene | Ours (600 rotating) | | 3DGS (100 static) | | 3DGS (660 static) | |
|-----------|------------------------|-------|----------------------|-------|----------------------|-------|
| | PSNR | LPIPS | PSNR | LPIPS | PSNR | LPIPS |
| Armadillo | 35.760 | 0.025 | 35.949 | 0.036 | 36.588 | 0.035 |
| Ficus | 34.227 | 0.007 | 34.001 | 0.008 | 35.207 | 0.007 |
| Flowers | 31.920 | 0.020 | 30.237 | 0.037 | 31.288 | 0.033 |
| Lego | 33.507 | 0.026 | 32.137 | 0.045 | 32.957 | 0.041 |
| Average | 33.853 | 0.020 | 33.081 | 0.032 | 34.010 | 0.029 |

Although it can reconstruct good geometries, the radiance (especially the shadow effects) is incorrectly predicted. In contrast, our method produces results that closely match the reference, thanks to the conditional radiance representation.

Studio box dataset. We further compare the rendering quality between our method and 3DGS on four scenes from the *studio box* datasets, which offer high-quality photographic lighting with less lighting variation. These scenes are chosen to cover several typical

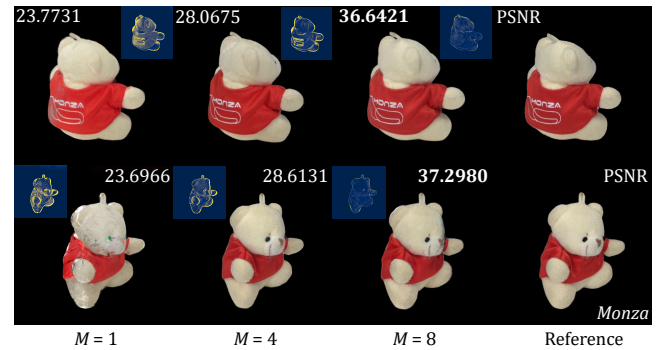


Fig. 7. The effect of the number of circles (M) in our pipeline. Given only one fixed camera position, we only observe one “diagonal line” in the view-light space, resulting in severe over-fitting. In practice, we choose $M = 8$ for our real datasets.

effects, including high specular, detailed fur, etc. Our method still surpasses 3DGS in all these scenarios, showing about 5 dB higher PSNR on average. While the quality of 3DGS has also been improved compared to the ones from the *default* datasets, it still suffers from missing specular highlights (top left) and over-blurred appearance (two scenes at the bottom), while our renderings preserve these details and better match the ground truth.

We provide results from synthetic datasets using our capturing pipeline but test with full static images (without any light rotations)

to compare the NVS quality. In this comparison, 3DGS uses ideally sampled fully static training images. We provide the rendering comparisons in Fig. 9 and quantitative results in Table 2. Our neural radiance representation achieves higher-quality renderings than that from 3DGS with a common setup (100 static images) and is still competitive with results of 3DGS from abundantly sampled static views (660 static images). Note that in practice, even for 600 images with rotating lights, we still need no more than 4 minutes to capture them, while capturing 100 high-quality static images already costs more than 3 minutes of difficult manual labor. In addition, our NVS quality can be further improved with another variant of our datasets. We describe and validate this in our supplementary.

5.4 More applications

Relighting with the neural representation. Since our method reconstructs a two-dimensional manifold, considering both the light rotations and different views, it naturally supports relighting with the same light but with different rotations. In Fig. 11, we showcase the rendered result under different light rotations. We use the *Rabbit* scene from the *default* dataset as an example. With varying lighting conditions, our rendered results exhibit overall reasonable lighting outcomes. Since it is difficult to achieve rotating light with a fixed camera in practice, we don't provide ground truths for comparison in this figure.

NVS with distilled SH representation. After selecting a lighting angle, our neural representation can be easily distilled into an SH representation. This way, it can fit existing 3DGS-based applications. In Fig. 5, we show the NVS results rendered with the distilled SHs under three different lighting rotations. The distilled SHs achieve close qualities to the results from our neural radiance representation, producing faithful NVS compared to the ground truth at the specified rotation angles. Note that we obtain all the results from only one training. A typical distillation process can finish within 3 minutes.

Relighting under novel light conditions. Our neural representation encodes the radiance field with multiple light conditions, which allows us to linearly combine different light rotations (e.g., front-lit and back-lit ones), achieving a fused light condition. In Fig. 6, we demonstrate the relighting results by combining the front-lit and the back-lit scenarios, with different lighting colors. The way, our method enables the creation of rich and diverse assets.

5.5 Ablation study

In our capture pipeline, we need to position the camera on a tripod in several locations, where this location number M is a crucial factor. To validate its influence, we provide an ablation study in Fig. 7 by setting different values of M with the *default* setup. For fairness, we keep the same total number of captures across the different setups (1, 4, and 8 locations). By comparison, increasing the number of locations improves the rendering quality. The main reason behind this phenomenon is that sparse locations lead to uneven sampling on the 2D manifold, which can lead to overfitting during optimization and hurting the rendering quality.

5.6 Discussion and limitations

More flexible relighting. Our capture pipeline enables relighting with different light rotations or a linear combination of various lighting conditions. However, our method still cannot fully or flexibly support relighting in entirely new environments. We will address this in future work.

Data processing. Our capture pipeline relies on COLMAP [Schönbberger and Frahm 2016] to calibrate our camera poses. However, the light condition changes during the capturing, which raises the difficulty of calibrating. While the current background removal can alleviate this issue, it might occasionally fail due to the capability of the large model. Therefore, either a COLMAP-free calibration or a more accurate background removal approach will further improve our capture quality.

Alternative NVS frameworks. We choose the basic 3DGS framework to validate the effectiveness of our capturing pipeline. However, there are still many advanced approaches that provide even higher NVS qualities. Their work is orthogonal to ours and our pipeline is flexible enough to fit into most of such advanced approaches.

6 CONCLUSION

In this paper, we have presented *Free Your Hands*, a lightweight object-capturing pipeline to reduce manual workload, standardize the acquisition process, and ensure repeatability. The proposed capture pipeline consists of a simple setup: a consumer turntable to hold the target object and a tripod to hold the camera. As the turntable rotates, we can easily capture hundreds of valid images in several minutes without hands-on effort. Then, we design a neural radiance representation conditioned on light rotations tailored for the captured images. Our capture pipeline can be integrated into both NeRF or 3DGS-based frameworks. We have demonstrated the effectiveness of our pipeline in the 3DGS-based framework across various applications, including NVS and relighting under different light rotations or combined lighting conditions, showing competitive quality in NVS and reasonable relighting effects.

There are still many potential future research directions. One promising avenue is to expand the neural radiance representation into a fully relightable manifold. Additionally, improving the NVS and relighting quality on some difficult types of objects, such as reflective or transparent ones, is also an interesting and challenging direction.

REFERENCES

- Benjamin Attal, Jia-Bin Huang, Christian Richardt, Michael Zollhöfer, Johannes Kopf, Matthew O’Toole, and Changil Kim. 2023. HyperReel: High-Fidelity 6-DoF Video With Ray-Conditioned Sampling. In *Proceedings of the IEEE/CVF Conference on Computer Vision and Pattern Recognition (CVPR)*. 16610–16620.
- Jonathan T Barron, Ben Mildenhall, Matthew Tancik, Peter Hedman, Ricardo Martin-Brualla, and Pratul P Srinivasan. 2021. Mip-nerf: A multiscale representation for anti-aliasing neural radiance fields. In *Proceedings of the IEEE/CVF International Conference on Computer Vision*. 5855–5864.
- Jonathan T Barron, Ben Mildenhall, Dor Verbin, Pratul P Srinivasan, and Peter Hedman. 2022. Mip-nerf 360: Unbounded anti-aliased neural radiance fields. In *Proceedings of the IEEE/CVF Conference on Computer Vision and Pattern Recognition*. 5470–5479.
- Jonathan T Barron, Ben Mildenhall, Dor Verbin, Pratul P Srinivasan, and Peter Hedman. 2023. Zip-NeRF: Anti-aliased grid-based neural radiance fields. *arXiv preprint arXiv:2304.06706* (2023).
- Sai Bi, Zexiang Xu, Pratul Srinivasan, Ben Mildenhall, Kalyan Sunkavalli, Miloš Hašan, Yannick Hold-Geoffroy, David Kriegman, and Ravi Ramamoorthi. 2020a. Neural reflectance fields for appearance acquisition. *arXiv preprint arXiv:2008.03824* (2020).
- Sai Bi, Zexiang Xu, Kalyan Sunkavalli, Miloš Hašan, Yannick Hold-Geoffroy, David Kriegman, and Ravi Ramamoorthi. 2020b. Deep reflectance volumes: Relightable reconstructions from multi-view photometric images. In *Computer Vision–ECCV 2020: 16th European Conference, Glasgow, UK, August 23–28, 2020, Proceedings, Part III* 16. Springer, 294–311.
- Sai Bi, Zexiang Xu, Kalyan Sunkavalli, David Kriegman, and Ravi Ramamoorthi. 2020c. Deep 3d capture: Geometry and reflectance from sparse multi-view images. In *Proceedings of the IEEE/CVF conference on computer vision and pattern recognition*. 5960–5969.
- Zoubin Bi, Yixun Zeng, Chong Zeng, Fan Pei, Xiang Feng, Kun Zhou, and Hongzhi Wu. 2024a. Gs3: Efficient relighting with triple gaussian splatting. In *SIGGRAPH Asia 2024 Conference Papers*. 1–12.
- Zoubin Bi, Yixun Zeng, Chong Zeng, Fan Pei, Xiang Feng, Kun Zhou, and Hongzhi Wu. 2024b. GS³: Efficient Relighting with Triple Gaussian Splatting. In *SIGGRAPH Asia 2024 Conference Papers*.
- Mark Boss, Varun Jampani, Raphael Braun, Ce Liu, Jonathan Barron, and Hendrik Lensch. 2021. Neural-pil: Neural pre-integrated lighting for reflectance decomposition. *Advances in Neural Information Processing Systems* 34 (2021), 10691–10704.
- David Charatan, Sizhe Lester Li, Andrea Tagliasacchi, and Vincent Sitzmann. 2024. pixelsplat: 3d gaussian splats from image pairs for scalable generalizable 3d reconstruction. In *Proceedings of the IEEE/CVF Conference on Computer Vision and Pattern Recognition*. 19457–19467.
- Anpei Chen, Zexiang Xu, Andreas Geiger, Jingyi Yu, and Hao Su. 2022. Tensorf: Tensorial radiance fields. In *European conference on computer vision*. Springer, 333–350.
- Yuedong Chen, Haoifei Xu, Chuanxia Zheng, Bohan Zhuang, Marc Pollefeys, Andreas Geiger, Tat-Jen Cham, and Jianfei Cai. 2025. MVSpLat: Efficient 3D Gaussian Splatting from Sparse Multi-view Images. In *Computer Vision – ECCV 2024*, Aleš Leonardis, Elisa Ricci, Stefan Roth, Olga Russakovsky, Torsten Sattler, and Gül Varol (Eds.). Springer Nature Switzerland, Cham, 370–386.
- Duan Gao, Guojun Chen, Yue Dong, Pieter Peers, Kun Xu, and Xin Tong. 2020. Deferred neural lighting: free-viewpoint relighting from unstructured photographs. *ACM Transactions on Graphics (TOG)* 39, 6 (2020), 1–15.
- Jian Gao, Chun Gu, Youtian Lin, Hao Zhu, Xun Cao, Li Zhang, and Yao Yao. 2023. Relightable 3d gaussian: Real-time point cloud relighting with brdf decomposition and ray tracing. *arXiv preprint arXiv:2311.16043* (2023).
- Richard Hartley and Andrew Zisserman. 2003. *Multiple view geometry in computer vision*.
- Haian Jin, Isabella Liu, Peijia Xu, Xiaoshuai Zhang, Songfang Han, Sai Bi, Xiaowei Zhou, Zexiang Xu, and Hao Su. 2023. Tensorf: Tensorial inverse rendering. In *Proceedings of the IEEE/CVF Conference on Computer Vision and Pattern Recognition*. 165–174.
- Kaizhang Kang, Zoubin Bi, Xiang Feng, Yican Dong, Kun Zhou, and Hongzhi Wu. 2023. Differentiable Dynamic Visible-Light Tomography. In *SIGGRAPH Asia 2023 Conference Papers*. 1–12.
- Bernhard Kerbl, Georgios Kopanas, Thomas Leimkühler, and George Drettakis. 2023. 3d gaussian splatting for real-time radiance field rendering. *ACM Transactions on Graphics (ToG)* 42, 4 (2023), 1–14.
- Zhihao Liang, Qi Zhang, Ying Feng, Ying Shan, and Kui Jia. 2024. Gs-ir: 3d gaussian splatting for inverse rendering. In *Proceedings of the IEEE/CVF Conference on Computer Vision and Pattern Recognition*. 21644–21653.
- Xi Liu, Chaoyi Zhou, and Siyu Huang. 2024. 3dgs-enhancer: Enhancing unbounded 3d gaussian splatting with view-consistent 2d diffusion priors. *arXiv preprint arXiv:2410.16266* (2024).
- Yuan Liu, Peng Wang, Cheng Lin, Xiaoxiao Long, Jiepeng Wang, Lingjie Liu, Taku Komura, and Wenping Wang. 2023. Nero: Neural geometry and brdf reconstruction of reflective objects from multiview images. *ACM Transactions on Graphics (TOG)* 42, 4 (2023), 1–22.
- Xiaohe Ma, Kaizhang Kang, Ruisheng Zhu, Hongzhi Wu, and Kun Zhou. 2021. Free-Form Scanning of Non-Planar Appearance with Neural Trace Photography. *ACM Trans. Graph.* 40, 4, Article 124 (July 2021), 13 pages. <https://doi.org/10.1145/3450626.3459679>
- Jiarui Meng, Haijie Li, Yanmin Wu, Qiankun Gao, Shuzhou Yang, Jian Zhang, and Siwei Ma. 2024. Mirror-3dgs: Incorporating mirror reflections into 3d gaussian splatting. *arXiv preprint arXiv:2404.01168* (2024).
- Ben Mildenhall, Pratul P Srinivasan, Matthew Tancik, Jonathan T Barron, Ravi Ramamoorthi, and Ren Ng. 2021. Nerf: Representing scenes as neural radiance fields for view synthesis. *Commun. ACM* (2021).
- Thomas Müller, Alex Evans, Christoph Schied, and Alexander Keller. 2022. Instant Neural Graphics Primitives with a Multiresolution Hash Encoding. *ACM Trans. Graph.* 41, 4, Article 102 (July 2022), 15 pages. <https://doi.org/10.1145/3528223.3530127>
- Krishna Mullia, Fujun Luan, Xin Sun, and Miloš Hašan. 2024. RNA: Relightable Neural Assets. *ACM Transactions on Graphics* (2024).
- Raul Mur-Artal, Jose Maria Martinez Montiel, and Juan D Tardos. 2015. ORB-SLAM: a versatile and accurate monocular SLAM system. *IEEE transactions on robotics* (2015).
- Nikhila Ravi, Valentin Gabeur, Yuan-Ting Hu, Ronghang Hu, Chaitanya Ryali, Tengyu Ma, Haitham Khedr, Roman Rädle, Chloe Rolland, Laura Gustafson, et al. 2024. Sam 2: Segment anything in images and videos. *arXiv preprint arXiv:2408.00714* (2024).
- Johannes L Schonberger and Jan-Michael Frahm. 2016. Structure-from-motion revisited. In *CVPR*.
- Johannes Lutz Schönberger and Jan-Michael Frahm. 2016. Structure-from-Motion Revisited. In *Conference on Computer Vision and Pattern Recognition (CVPR)*.
- Takafumi Taketomi, Hideaki Uchiyama, and Sei Ikeda. 2017. Visual SLAM algorithms: A survey from 2010 to 2016. *IPST Transactions on Computer Vision and Applications* 9, 1 (2017), 1–11.
- Dor Verbin, Peter Hedman, Ben Mildenhall, Todd Zickler, Jonathan T Barron, and Pratul P Srinivasan. 2022. Ref-nerf: Structured view-dependent appearance for neural radiance fields. In *2022 IEEE/CVF Conference on Computer Vision and Pattern Recognition (CVPR)*. IEEE, 5481–5490.
- Zhou Wang, Alan C Bovik, Hamid R Sheikh, and Eero P Simoncelli. 2004. Image quality assessment: from error visibility to structural similarity. (2004).
- Zirui Wang, Shangzhe Wu, Weidi Xie, Min Chen, and Victor Adrian Prisacariu. 2021. NeRF-: Neural radiance fields without known camera parameters. *arXiv preprint arXiv:2102.07064* (2021).
- Yao Yao, Jingyang Zhang, Jingbo Liu, Yihang Qu, Tian Fang, David McKinnon, Yanghai Tsing, and Long Quan. 2022. Neif: Neural incident light field for physically-based material estimation. In *European Conference on Computer Vision*. Springer, 700–716.
- Sheng Ye, Yuze He, Matthieu Lin, Jenny Sheng, Ruoyu Fan, Yiheng Han, Yubin Hu, Ran Yi, Yu-Hui Wen, Yong-Jin Liu, et al. 2024. PVP-Recon: Progressive View Planning via Warping Consistency for Sparse-View Surface Reconstruction. *ACM Transactions on Graphics (TOG)* 43, 6 (2024), 1–13.
- Mulin Yu, Tao Lu, Linning Xu, Lihan Jiang, Yuanbo Xiangli, and Bo Dai. 2024. GsdF: 3dgs meets sdf for improved rendering and reconstruction. *arXiv preprint arXiv:2403.16964* (2024).
- Chong Zeng, Guojun Chen, Yue Dong, Pieter Peers, Hongzhi Wu, and Xin Tong. 2023. Relighting neural radiance fields with shadow and highlight hints. In *ACM SIGGRAPH 2023 Conference Proceedings*. 1–11.
- Kai Zhang, Fujun Luan, Qianqian Wang, Kavita Bala, and Noah Snavely. 2021. PhysG: Inverse rendering with spherical gaussians for physics-based material editing and relighting. In *Proceedings of the IEEE/CVF Conference on Computer Vision and Pattern Recognition*. 5453–5462.
- Kai Zhang, Gernot Riegler, Noah Snavely, and Vladlen Koltun. 2020. Nerf++: Analyzing and improving neural radiance fields. *arXiv preprint arXiv:2010.07492* (2020).
- Richard Zhang, Phillip Isola, Alexei A Efros, Eli Shechtman, and Oliver Wang. 2018. The unreasonable effectiveness of deep features as a perceptual metric.

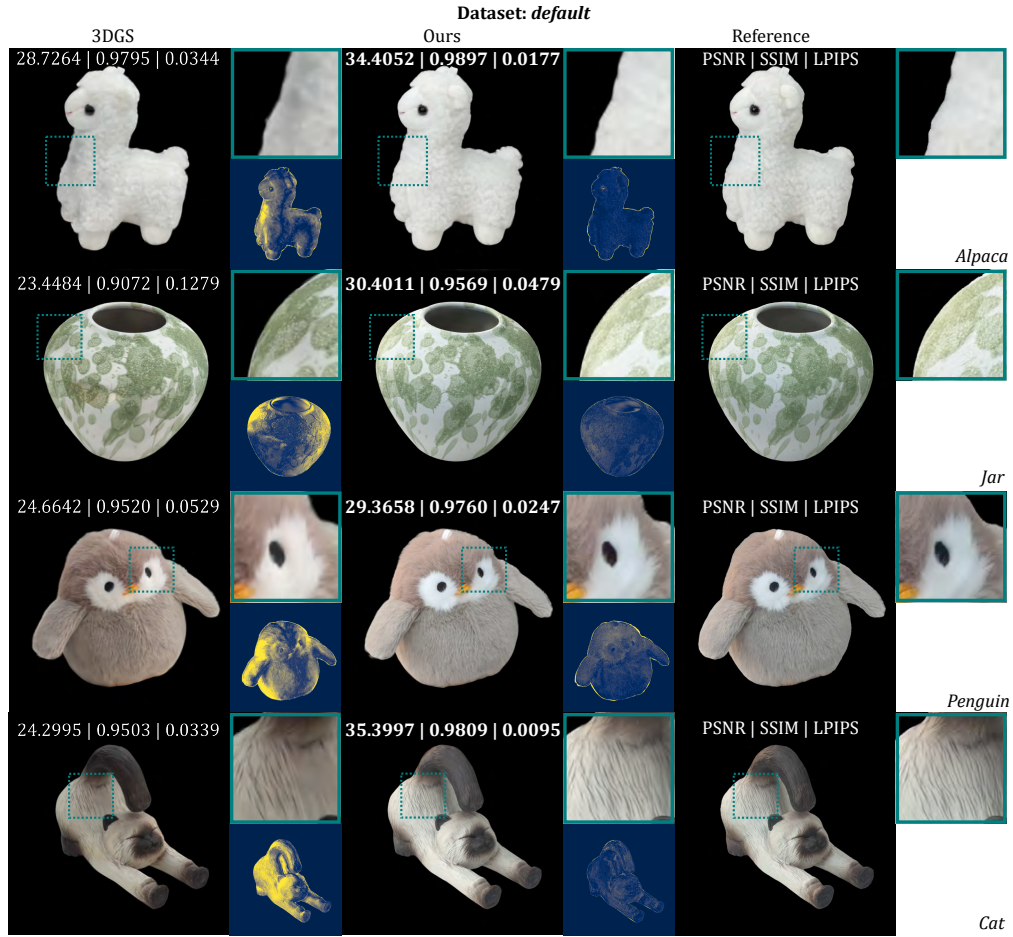


Fig. 8. Comparison of rendering results with novel views and light rotations by our neural radiance manifold prediction and 3DGS on *default* datasets. The best results are marked as **bold**. 3DGS cannot handle the rotating light conditions, resulting in wrongly predicted shadow/light effects. In contrast, our pipeline provides closer results to the reference.

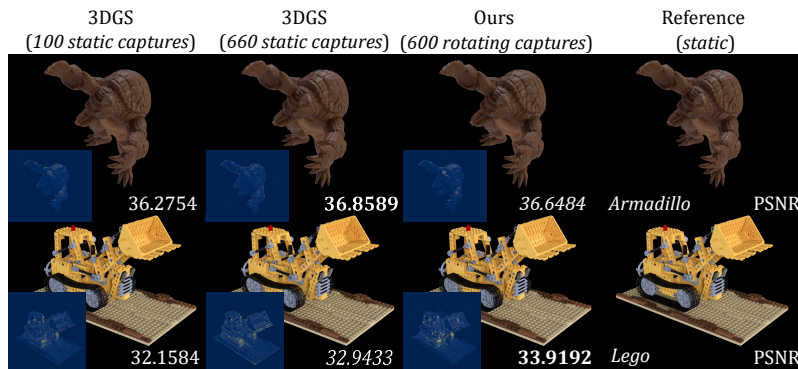


Fig. 9. The NVS comparison on synthetic datasets. Here 3DGS uses ideally sampled fully static training images. The best/second-best results are marked as **bold/italic**. All testing images are also static (without any light rotations). Our neural radiance representation achieves high-quality renderings, and is competitive with results of 3DGS from ideally sampled static views.

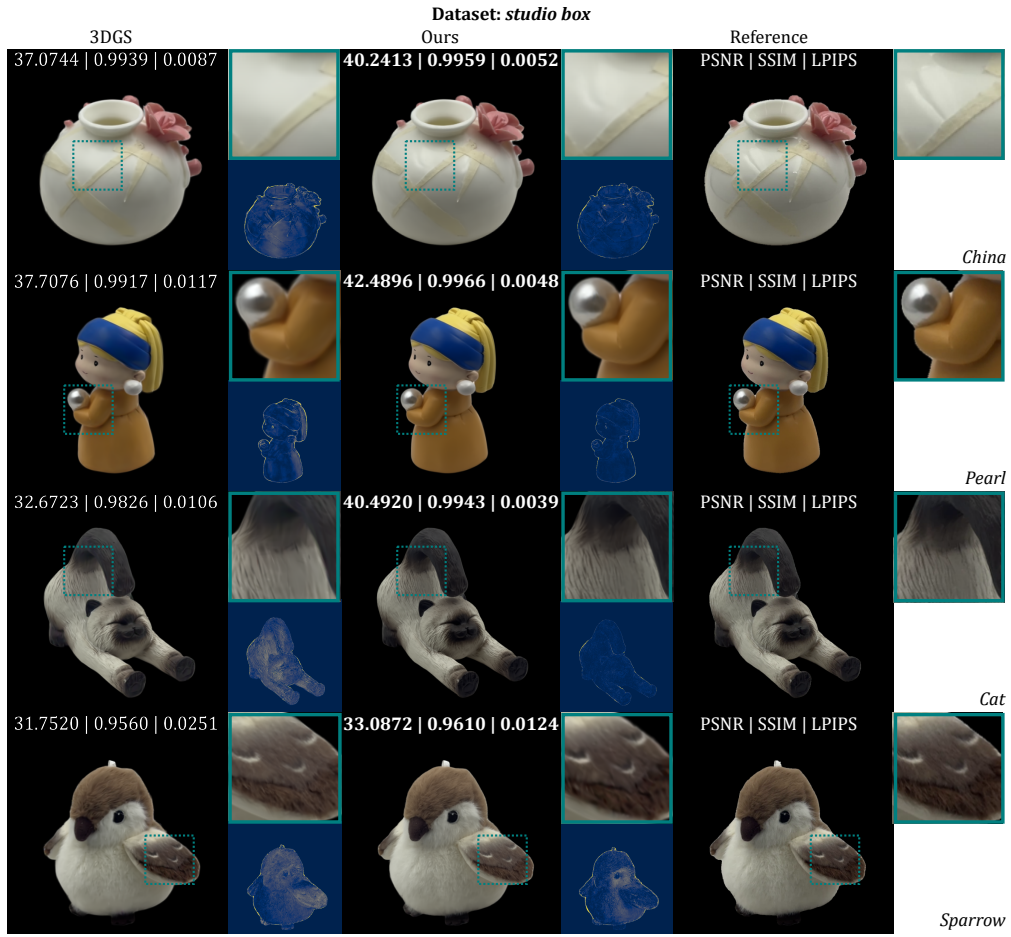


Fig. 10. The rendering results with novel views and light rotations on the *studio box* datasets with high-quality photographic studio lights. The best results are marked as **bold**. Both 3DGS and our method can achieve plausible renderings, while our quality is still higher.

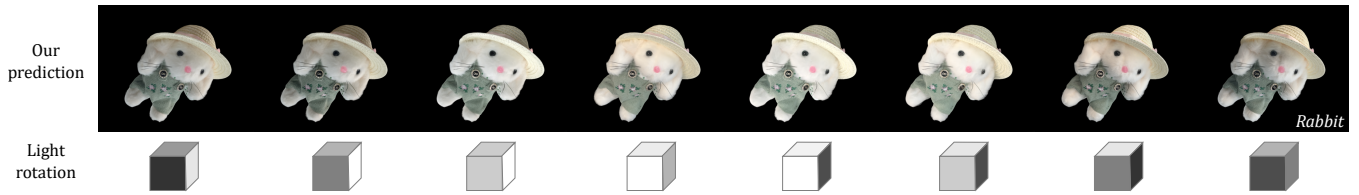


Fig. 11. The rendering results of our model from a novel view and novel light rotations. Our method can effectively predict reasonable light transition when light rotates, as our light-conditioned neural representation is learned based on samples from multiple light conditions.

Supplementary Materials:

Free Your Hands: Lightweight Relightable Turntable Capture Pipeline

JIAHUI FAN, Nanjing University of Science and Technology, China
FUJUN LUAN, Adobe Research, USA
JIAN YANG[†], Nanjing University of Science and Technology, China
MILOŠ HAŠAN, Adobe Research, USA
BEIBEI WANG[‡], Nanjing University, China

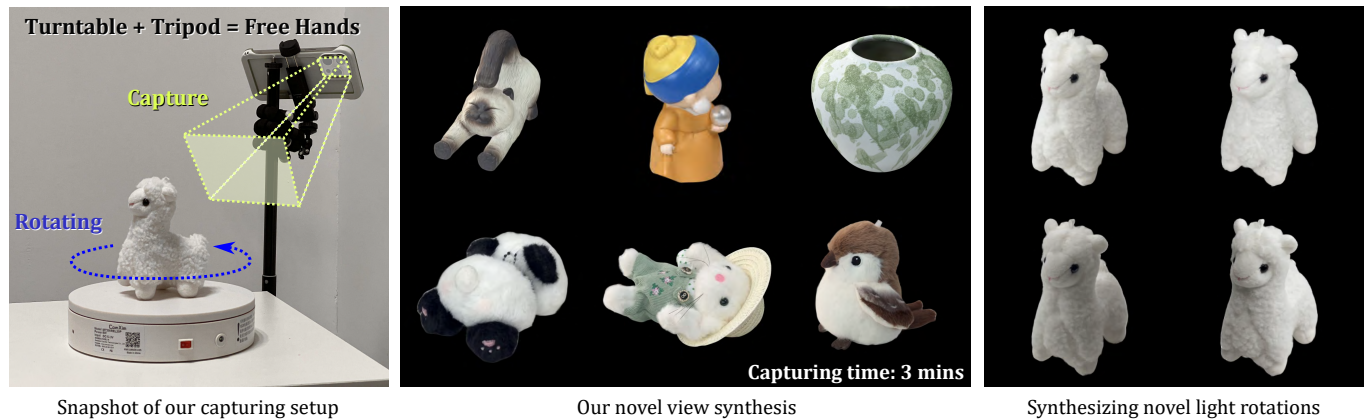


Fig. 12. We present a lightweight object-capturing pipeline to reduce the workload and standardize the acquisition procedure. We use a consumer turntable to carry the object and a tripod to hold the camera (left), automatically capturing dense samples from various views and lighting conditions. This way, we easily obtain hundreds of high-quality captures within 3 minutes. We develop a conditional neural radiance representation, achieving high-quality novel view synthesis (middle). With this representation, we can further synthesize results under novel views and light rotations (right).

Novel view synthesis (NVS) from multiple captured photos of an object is a widely studied problem. Achieving high quality typically requires dense sampling of input views, which can lead to frustrating and tedious manual labor. Manually positioning cameras to maintain an optimal desired distribution can be difficult for humans, and if a good distribution is found, it is not easy to replicate. Additionally, the captured data can suffer from motion blur and defocus due to human error. In this paper, we present a lightweight object capture pipeline to reduce the manual workload and standardize the acquisition setup. We use a consumer turntable to carry the object and a tripod to hold the camera. As the turntable rotates, we automatically capture dense samples from various views and lighting conditions; we can repeat this for several camera positions. This way, we can easily capture hundreds of valid images in several minutes without hands-on effort. However, in the object reference frame, the light conditions vary; this is harmful to a standard NVS method like 3D Gaussian splatting (3DGS) which assumes fixed lighting. We design a neural radiance representation conditioned on light rotations, which addresses this issue and allows relightability as an additional benefit. We demonstrate our pipeline using 3DGS as the underlying framework, achieving competitive quality compared to previous methods with exhaustive acquisition and showcasing its potential for relighting and harmonization tasks.

[†] Corresponding authors. Email: csjiang@njust.edu.cn.

[‡] Corresponding authors. Email: beibei.wang@nju.edu.cn.

Authors' addresses: Jiahui Fan, Nanjing University of Science and Technology, China, fjh@njust.edu.cn; Fujun Luan, Adobe Research, USA, fluan@adobe.com; Jian Yang[†], Nanjing University of Science and Technology, China, csjiang@njust.edu.cn; Miloš Hašan, Adobe Research, USA, milos.hasan@gmail.com; Beibei Wang[‡], Nanjing University, China, beibei.wang@njust.edu.cn.

In the main paper, we have proposed *Free Your Hands*, a lightweight relightable object-capturing pipeline with a turntable, allowing for NVS and relighting. We have also introduced a novel formulation of NVS problems and provided two versions of datasets that contain 17 real-world objects. In this supplementary, we introduce and discuss another variant of our proposed dataset with 20 extra sparse static captures as input.

Our pipeline captures images under rotating light conditions and achieves rendering with novel views and light rotations simultaneously. However, when focusing on NVS (without any light rotations), we can further improve the qualities by adding a few extra samples at the target fixed light rotation. Therefore, we also present a variant of our dataset with 20 extra images captured under the static environment light (called the *+20 static* dataset). Theoretically, more extra static captures bring higher NVS quality at the target light condition. In practice, to balance the time cost and quality, we capture 20 extra static images.

We show the effect of these extra sparse static captures in Fig. 13, and also provide the quantitative results on our *+20 static* datasets, compared to the *default* ones in Table 3. Generally, The *+20 static* datasets give similar qualities compared to *default* datasets on such testing sets since the extra captures will not help the rendering with novel light rotations, but only for the static NVS.

To validate the improvement in NVS, we also provide results on synthetic datasets with *static images* as the testing set. We use *+20*

Table 3. Rendering qualities with novel view and light rotation from our neural radiance representation on different datasets. The results are evaluated in PSNR (\uparrow), SSIM (\uparrow) and LPIPS (\downarrow). The best/second-best/third-best results are colored in red / yellow . Our neural radiance representation outperforms 3DGS on both variants of datasets.

| Scene | Default dataset (3 minutes) (See the main paper) | | | | | | +20 static dataset (3.7 minutes) (Fig.13) | | | | | |
|------------|--------------------------------------------------|--------|--------|---------|--------|--------|-------------------------------------------|--------|--------|---------|--------|--------|
| | Ours | | | 3DGS | | | Ours | | | 3DGS | | |
| | PSNR | SSIM | LPIPS | PSNR | SSIM | LPIPS | PSNR | SSIM | LPIPS | PSNR | SSIM | LPIPS |
| Alpaca | 33.7039 | 0.9894 | 0.0169 | 29.6081 | 0.9806 | 0.0323 | 34.2296 | 0.9906 | 0.0161 | 29.1272 | 0.9802 | 0.0329 |
| Cat | 30.9368 | 0.9835 | 0.0109 | 26.0663 | 0.9555 | 0.0356 | 33.1386 | 0.9828 | 0.0114 | 26.0425 | 0.9535 | 0.0415 |
| China | 34.2610 | 0.9897 | 0.0090 | 30.7809 | 0.9844 | 0.0146 | 35.3399 | 0.9903 | 0.0095 | 30.3217 | 0.9835 | 0.0153 |
| Controller | 30.4726 | 0.9761 | 0.0209 | 25.2222 | 0.9659 | 0.0345 | 30.7255 | 0.9767 | 0.0206 | 24.5290 | 0.9648 | 0.0356 |
| Dinosaur | 36.0936 | 0.9928 | 0.0065 | 32.5989 | 0.9883 | 0.0123 | 36.3225 | 0.9930 | 0.0062 | 33.5739 | 0.9889 | 0.0125 |
| Dolphin | 39.0878 | 0.9961 | 0.0048 | 34.1935 | 0.9924 | 0.0086 | 39.1236 | 0.9959 | 0.0050 | 33.6032 | 0.9920 | 0.0091 |
| Jar | 29.3733 | 0.9553 | 0.0484 | 23.6761 | 0.9101 | 0.1196 | 29.8483 | 0.9484 | 0.0596 | 23.7533 | 0.9012 | 0.1390 |
| Monza | 36.5302 | 0.9926 | 0.0054 | 29.6788 | 0.9844 | 0.0104 | 36.5283 | 0.9928 | 0.0050 | 29.4366 | 0.9841 | 0.0101 |
| Panda | 29.1212 | 0.9780 | 0.0288 | 25.7316 | 0.9628 | 0.0525 | 28.6421 | 0.9778 | 0.0288 | 26.4826 | 0.9660 | 0.0517 |
| Pearl | 38.0879 | 0.9917 | 0.0070 | 30.4644 | 0.9834 | 0.0140 | 37.5966 | 0.9921 | 0.0066 | 30.5545 | 0.9839 | 0.0143 |
| Penguin | 28.9595 | 0.9698 | 0.0290 | 23.9183 | 0.9453 | 0.0598 | 29.5938 | 0.9699 | 0.0295 | 23.9765 | 0.9467 | 0.0600 |
| Pine | 25.6992 | 0.9451 | 0.0421 | 21.7535 | 0.8820 | 0.0881 | 29.2246 | 0.9504 | 0.0375 | 21.8756 | 0.8822 | 0.0922 |
| Rabbit | 31.6668 | 0.9760 | 0.0200 | 29.4303 | 0.9592 | 0.0413 | 32.1203 | 0.9823 | 0.0198 | 29.8564 | 0.9657 | 0.0409 |
| Rider | 28.6987 | 0.9486 | 0.0345 | 25.3948 | 0.9275 | 0.0535 | 28.5096 | 0.9498 | 0.0346 | 25.6186 | 0.9280 | 0.0538 |
| RiderSmall | 37.5932 | 0.9924 | 0.0053 | 31.0377 | 0.9830 | 0.0115 | 37.2683 | 0.9922 | 0.0056 | 31.0191 | 0.9817 | 0.0128 |
| Sparrow | 29.7554 | 0.9720 | 0.0309 | 25.6735 | 0.9593 | 0.0531 | 29.4498 | 0.9715 | 0.0316 | 25.7855 | 0.9596 | 0.0541 |
| Tuan | 31.5752 | 0.9827 | 0.0234 | 23.9322 | 0.9693 | 0.0439 | 31.3717 | 0.9827 | 0.0239 | 23.6291 | 0.9688 | 0.0447 |
| Average | 32.4968 | 0.9785 | 0.0202 | 27.4832 | 0.9609 | 0.0403 | 32.8843 | 0.9788 | 0.0206 | 27.5991 | 0.9606 | 0.0424 |

Table 4. The NVS qualities with different numbers of extra sparse static captures as input. All results are evaluated in PSNR (\uparrow), SSIM (\uparrow), and LPIPS (\downarrow), and best/second-best/third-best results are marked in red / orange / yellow . Note that in this figure, the testing set is without any light rotations. By adding sparse captures with the targeted light condition, the NVS quality of our pipeline can be further improved, even surpassing 3DGS with the ideal exhaustive acquisition. However, we only need no more than 4 minutes in practice to obtain such a dataset, while it will take more than 20 minutes for a hand-held camera to finish the ordinary capturing.

| Scene | Ours (600 rotating) | | | Ours (+10 static) | | | Ours (+30 static) | | | 3DGS (100 static) | | | 3DGS (660 static) | | |
|-----------|---------------------|-------|-------|-------------------|-------|-------|-------------------|-------|-------|-------------------|-------|-------|-------------------|-------|-------|
| | PSNR | SSIM | LPIPS | PSNR | SSIM | LPIPS | PSNR | SSIM | LPIPS | PSNR | SSIM | LPIPS | PSNR | SSIM | LPIPS |
| Armadillo | 35.760 | 0.968 | 0.025 | 36.812 | 0.971 | 0.023 | 38.175 | 0.974 | 0.021 | 35.949 | 0.963 | 0.036 | 36.588 | 0.965 | 0.035 |
| Ficus | 34.227 | 0.984 | 0.007 | 34.896 | 0.986 | 0.006 | 35.900 | 0.988 | 0.005 | 34.001 | 0.984 | 0.008 | 35.207 | 0.988 | 0.007 |
| Flowers | 31.920 | 0.976 | 0.020 | 32.434 | 0.978 | 0.019 | 32.657 | 0.979 | 0.019 | 30.237 | 0.963 | 0.037 | 31.288 | 0.970 | 0.033 |
| Lego | 33.507 | 0.959 | 0.026 | 34.077 | 0.963 | 0.024 | 35.398 | 0.971 | 0.019 | 32.137 | 0.951 | 0.045 | 32.957 | 0.958 | 0.041 |
| Average | 33.853 | 0.972 | 0.020 | 34.555 | 0.974 | 0.018 | 35.532 | 0.978 | 0.016 | 33.081 | 0.965 | 0.032 | 34.010 | 0.970 | 0.029 |

static for real-world datasets and use +10/30 static synthetic datasets to demonstrate the effectiveness of extra static captures and show the impact of the number of static captures. In practice, even for +30 static, we still only need about 1 minute extra work time (4 minutes in total), while the hand-held camera can only capture about 120 valid static images in the same amount of time.

In Fig. 14, we show the impact of extra static captures in the final NVS quality, and quantitative results are also provided in Table 4. Our NVS result from rotating captures is closer to the ground truth compared to a standard 3DGS capture (from 100 static images), and stays competitive with 3DGS using the ideal exhaustive acquisition (660 static images). With extra static captures,

we can further improve our NVS quality, outperforming 3DGS even with 660 static captures. Additionally provided static captures significantly improve our NVS quality, since the network can focus more on the specific 1D sample space than the global manifold. In contrast, 3DGS only gets marginal improvement from extra captures. We only demonstrate this on synthetic scenes, since the ideal high-quality and reasonably sampled static captures for 3DGS are difficult to collect in practice. Our method can significantly benefit from sparse additional samples under the desired light condition without much extra workload and time cost.

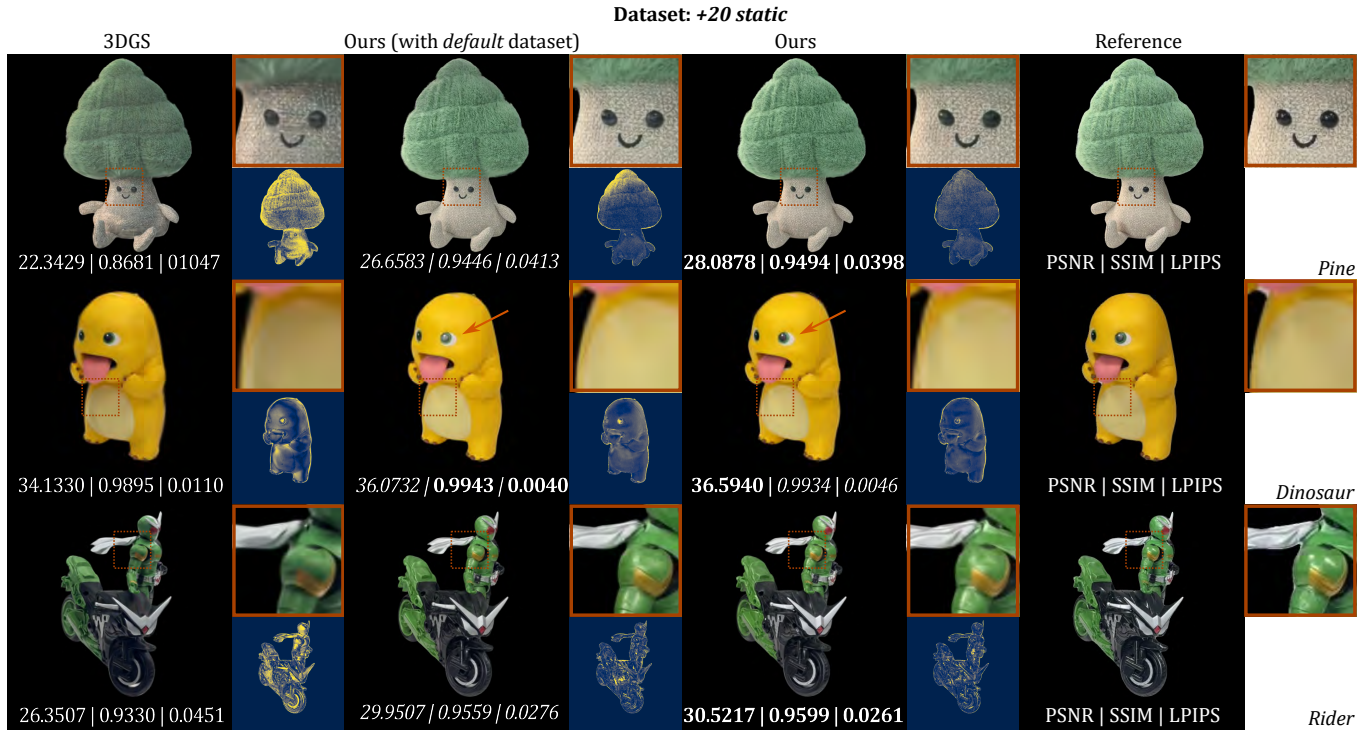


Fig. 13. The rendering results with novel views and light rotations on +20 static datasets. The best/second-best results are marked as **bold/italic**. Compared to the *default* setting, Our NVS quality can be further improved on such datasets, while 3DGS still has incorrect shadow effects.

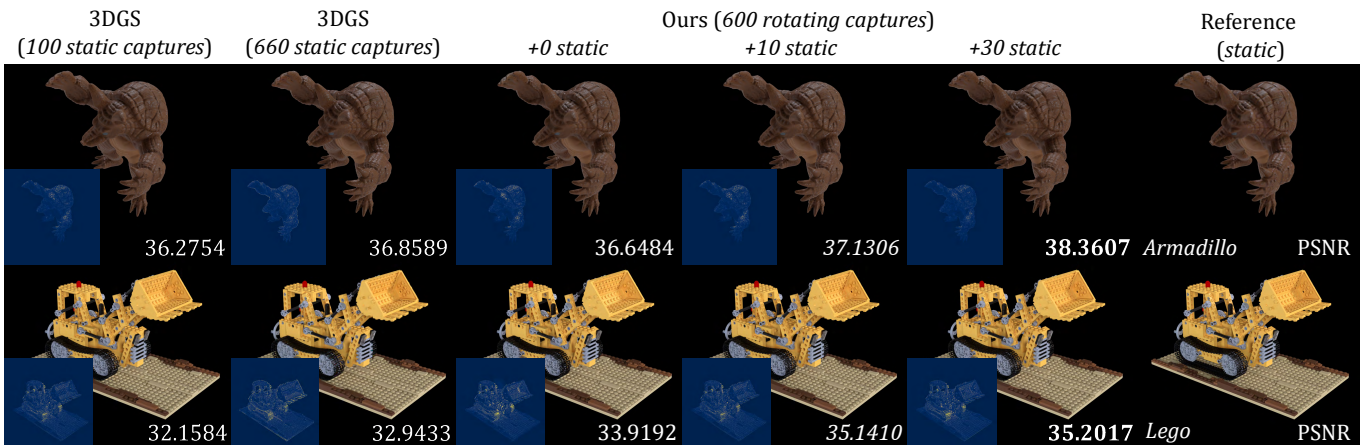


Fig. 14. The ablation on the impact of extra sparse static captures. Our method can significantly benefit from sparse additional samples under the desired light conditions, and still beat the quality of 3DGS, despite providing as many uniformly sampled ideal captures under a static light condition for them. Note that in this figure, all references are with the static lighting (i.e., NVS without any light rotations).